LETTERS

Laser acceleration of quasi-monoenergetic MeV ion beams

B. M. Hegelich[1], B. J. Albright[1], J. Cobble[1], K. Flippo[1], S. Letzring[1], M. Paffett[1], H. Ruhl[2], J. Schreiber[3,4], R. K. Schulze[1] & J. C. Fernández[1]

Acceleration of particles by intense laser–plasma interactions represents a rapidly evolving field of interest, as highlighted by the recent demonstration[1–4] of laser-driven relativistic beams of monoenergetic electrons. Ultrahigh-intensity lasers can produce accelerating fields of 10 TV m^{-1} (1 TV = 10^{12} V), surpassing those in conventional accelerators by six orders of magnitude. Laser-driven ions with energies of several MeV per nucleon have also been produced[5–9]. Such ion beams exhibit unprecedented characteristics—short pulse lengths, high currents and low transverse emittance[10]—but their exponential energy spectra have almost 100% energy spread. This large energy spread, which is a consequence of the experimental conditions used to date, remains the biggest impediment to the wider use of this technology. Here we report the production of quasi-monoenergetic laser-driven C^{5+} ions with a vastly reduced energy spread of 17%. The ions have a mean energy of 3 MeV per nucleon (full-width at half-maximum ~0.5 MeV per nucleon) and a longitudinal emittance of less than 2 × 10^{-6} eV s for pulse durations shorter than 1 ps. Such laser-driven, high-current, quasi-monoenergetic ion sources may enable significant advances in the development of compact MeV ion accelerators[11], new diagnostics[12,13], medical physics[14], inertial confinement fusion and fast ignition[15–17].

An ultrahigh-intensity laser ($I\lambda^2 > 10^{18}$ W cm^{-2} μm^{-2}, where I is intensity and λ is wavelength) incident on a target accelerates a large number of electrons to multi-MeV energies[18,19]. These electrons traverse typical thin foil targets and set up a very strong electrostatic field exceeding 1 TV m^{-1}. This field ionizes the rear surface and accelerates ions to energies of many MeV. This process is known as target normal sheath acceleration (TNSA)[5]. Experiments have demonstrated acceleration of protons to more than 60 MeV (ref. 8), fluorine ions to above 100 MeV (ref. 6) and high-Z palladium ions up to 225 MeV (ref. 20), that is, more than 2 MeV per nucleon. These ion beams have a much lower transverse temperature and a much shorter duration and a much higher current than those from conventional accelerators. These unique characteristics make them ideal candidates for a number of experiments not feasible otherwise.

Owing to their short pulse length and high energy content, the ion beams can heat macroscopic amounts of matter to more than 10^6 °C before the matter can expand[21], thereby creating conditions of high temperature and density only found in the interior of stars. Conversely they can also be used as a probe to investigate ion transport and stopping in a hot, dense plasma before it has time to disassemble. Conventional accelerators are hard pressed to deliver enough particles in the available ~ps time window to make high-quality measurements feasible. These are but two examples where the high current and short pulse duration are the key to an otherwise impossible experiment. More examples can be found in nuclear physics, fusion research and other areas—examples are the synthesis of neutron rich nuclei or the measurement of fusion cross-sections in supernova-like hot, dense plasma conditions. The much higher beam current and the much lower emittance of the laser-driven ion beams make them a promising candidate for advanced accelerator concepts.

Today, a standard linear accelerator that matches the MeV/u energy level (with u being the atomic mass unit) of these laser-driven ions is ~100 m long. In contrast, the laser fits in a large room and accelerates the ions to MeV/u over just 10 μm. The low duty-cycle in present experiments is a limitation that is likely to be mitigated by the next generation of high-power lasers, currently under development. However, the major difficulty with all the TNSA and other laser-driven ion-acceleration mechanisms[9,22] has been the resulting maxwellian energy distribution, with a typical 100% energy spread[6,8,9]. All the above-mentioned applications would benefit greatly from a narrower energy distribution, centred about a specific value.

We report here a laser-driven quasi-monoenergetic ion beam, a

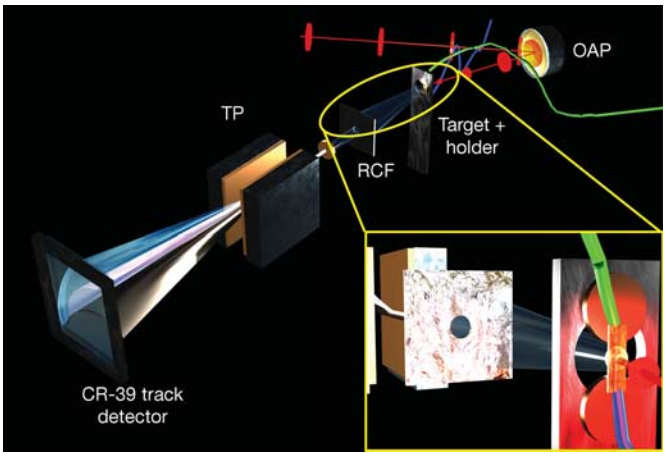

Figure 1 | Experimental set-up. A short, high-intensity laser pulse is focused on a thin metal foil target by an off-axis parabolic mirror (OAP). The red line shows the laser beam axis, and the red disks represent the laser pulse travelling along that axis and getting focused down by the OAP. Two wires (green and blue) are attached to the target, pass a current through it and heat it to ~1,100 K to remove contaminants. Ions are accelerated at the target rear surface and are detected by a stack of radiochromic film (RCF) and a Thomson parabola (TP) spectrometer using CR-39 track detectors. The inset shows an enlarged frontside view of the target, with the target and the green and blue wires being in the lower right corner and the RCF and TP detectors in the upper left.

[1]Los Alamos National Laboratory, Los Alamos, New Mexico 87545, USA. [2]University of Nevada, Reno, Nevada 89557, USA. [3]Ludwig-Maximilian-Universitaet Muenchen, [4]Max-Planck-Institüt für Quantenoptik, Garching 85748, Germany.

C^{5+} beam created in the interaction of a 20 TW/0.8 ps laser pulse with a solid target. A simple schematic illustrating the process can be found in Supplementary Information (sections SI_1 and SI_2). The experiments were performed at the LANL Trident laser facility. The experimental set-up is shown in Fig. 1 (for details see Methods), and a time-integrated photograph of an actual laser shot is shown in Supplementary Information section SI_3. The monoenergetic signature is the direct result of a fundamentally different target composition employed in these experiments. In TNSA, the ions with the highest charge-to-mass ratio dominate the acceleration, gaining the most energy. Given typical vacuum conditions of $\sim 10^{-6}$ mbar, surface target contaminants containing protons are always present. These protons have the largest charge-to-mass ratio by at least a factor of 2. Controlled treatment of foil targets before irradiation with the ultrahigh-intensity laser reduces adsorbed and absorbed proton contaminants to an unobservable level, allowing higher-Z ions to be the dominant species[6]. Using the right treatment parameters and target materials, a thin source layer of just a few monolayers can be formed by catalytic processes.

Specifically, we have demonstrated the acceleration of C^{5+} and C^{6+} from an ultrathin layer of graphitic carbon, formed from catalytic decomposition of adsorbed hydrocarbon impurities on a 20 μm palladium foil. Unlike the low-energy lasers which are used for electron acceleration[2–4], which have a high repetition rate and allow the taking of many shots to obtain good statistics, ion acceleration requires higher energy lasers which are single shot in nature. The number of shots is extremely limited and fluctuations in the laser parameters further complicate obtaining good statistics. However, five shots exhibiting monoenergetic carbon ions have been observed in two separate campaigns months apart, and another ten shots showing indication of monoenergetic ions are still being analysed. Figure 2 shows the measured C^{5+} spectrum (black curve) with the lowest ratio $\Delta E/E$ of ~17%, where E is the mean energy of the C^{5+} ions and ΔE is their energy spread. It also shows the corresponding highest substrate charge state Pd^{22+} (blue). Having the highest charge-to-mass ratio of 0.42, the C^{5+} is dominantly accelerated. Owing to the extremely small spatial extent of the carbon layer and its localization at the rear surface, all of the carbon ions are accelerated at once at the peak of the accelerating field, leading to the monoenergetic ion pulse. After all carbon ions are accelerated, the field is still very strong and only moderately screened by the carbon, therefore the next highest charge-to-mass ratio ion—that is, Pd^{22+} with a charge-to-mass ratio of 0.2—is now dominantly accelerated and gains a large fraction of the energy before the field decays and lower Pd charge states are created and accelerated.

For the purpose of this Letter we limit our discussion to the two dominant charge states, which together contain ~20% of the total integrated ion energy and have a bearing on the results reported here. The leading short bunch of C^{5+} ions shows a monoenergetic energy distribution with a mean energy of $E \approx 36$ MeV, that is, 3 MeV per nucleon and a full-width at half-maximum of 0.5 MeV per nucleon. We infer that the accelerated C^{5+} ion bunch has a longitudinal emittance of $\varepsilon_l < 2 \times 10^{-6}\,\pi$ eV s, improving on conventional high-current accelerators by orders of magnitude. Also, in contrast to the Pd and to any previous measurements, no lower C charge states are present. Closer analysis reveals important differences in the acceleration mechanism for the Pd substrate ions and the C ions from the source surface layer. Whereas the substrate ions have a typical exponential spectrum, the C ions are monoenergetic.

The small energy spread of the observed carbon ions can be understood from consideration of quasi-neutral ($n_e = Z_{Pd} n_{Pd}$), adiabatic expansion in one dimension (1D) of a palladium substrate coated by a very thin film of carbon. (Here n_e is the electron density, n_{Pd} the palladium density and Z_{Pd} the mean palladium charge state.) The electric field obeys $eE \approx -m_e n_e^{-1} \partial_x \int dv\, v^2 (f_e - Z_{Pd} f_{Pd})$, with f_e and f_{Pd} the distribution functions of electrons and palladium ions, e the elementary charge, m_e the electron mass and v velocity. Such a plasma column will expand with sound speed c_s to characteristic size $L^2(t) = L_0^2(1 + t^2 c_s^2 / L_0^2)$. The ion and electron temperatures will therefore decrease by a factor $L_0/L(t)$, which leads to an electric field $eE \approx x c_s^2 m_{Pd} Z_{Pd}^{-2} L^{-2}$, where m_{Pd} is the atomic mass of palladium. This field leads to an acceleration $d^2x_C/dt^2 = r x_C c_s^2 L^{-2}$ of the carbon ions, with x_C being the spatial coordinate of the carbon ions. The dynamics of the layer are characterized by r, the ratio of charge-to-mass ratios of C to Pd ions: for $r \gg 1$, the carbon layer detaches from the substrate at early time and propagates ahead of it as a directed bunch. For $r < 1$, the substrate overtakes the C layer and flow instabilities may arise. With an average Pd charge state $Z_{eff,Pd} \approx 7$, one obtains $r = 6.3$, predicting a clean separation of

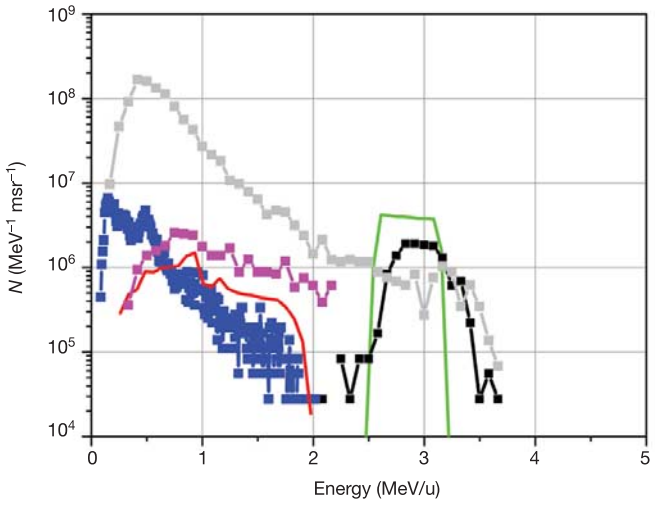

Figure 2 | Monoenergetic carbon ions from a 20 μm palladium substrate. The curves show ion number (N) over energy per nucleon (MeV/u). The black curve shows the spectra of the measured C^{5+} ions, the blue curve shows the dominant substrate charge state Pd^{22+}. The green and the red curves are simulations obtained using the 1D-hybrid-code BILBO, showing the simulated C^{5+} and Pd^{21+} spectra, respectively. The grey curve shows the dominant C^{4+}signal from a heated W target, and the magenta trace shows the C^{5+} signal from a cold Pd target. In these last two cases, the targets have a thick layer of carbon contaminants and do not form a monolayer source. The resulting carbon signals are therefore exponential and show lower numbers in the high-energy range. The errors are: $dN \leq 1\%$ statistical accuracy, and $dE \leq 2\%$ for C and $dE \leq 4.5\%$ for Pd.

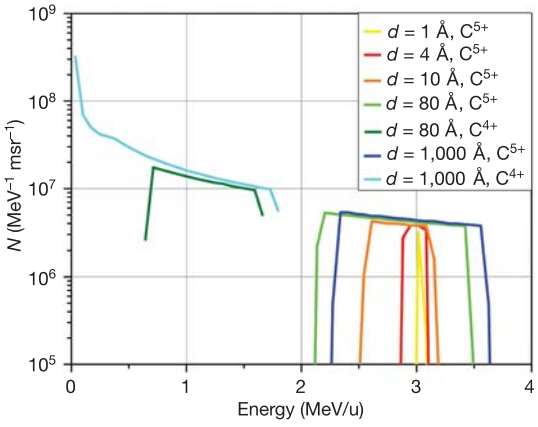

Figure 3 | Changing the thickness of the carbon source layer leads to a change in the energy spectrum in the BILBO simulations. Decreasing the layer thickness (d) causes the spectrum to become more monoenergetic. Increasing the layer thickness leads to a broader distribution and ultimately the appearance of lower charge states and a maxwellian spectrum.

the carbon ions from the substrate. Esirkepov *et al.*[23] have also examined the problem of monoenergetic ion acceleration, but their model relies explicitly upon finite transverse extent of the target and is not applicable to the TNSA scenario we find in our experiments.

In order to improve our understanding and our predictive capability, we developed a numerical model that simulates the ionization and acceleration physics. Full *ab initio* simulations with the required dynamics and sufficiently low noise levels to faithfully capture the ionization kinetics are not feasible, so we have focused on a reduced model that takes into account the essential physics. This 1D-hybrid model BILBO (backside ion lagrangian blow-off) uses a relativistic Boltzmann fluid model of the electrons and represents ions as kinetic simulation particles. This model has been explicitly designed to implement TNSA[5] in a heterogeneous mixture of ionization species and ion types. In our simulations, a thin layer of carbon (1–1,000 Å) with areal density $\rho = 5 \times 10^{-10}$–$5 \times 10^{-7}\,\mathrm{g\,cm^{-2}}$ is placed on the surface of a palladium foil of solid density $\rho = 12.16\,\mathrm{g\,cm^{3}}$ and a thickness of 20 μm. Using parameters matched to the experiment (see Methods), we are able to reproduce the experimental results.

Figure 2 shows the energy spectra of the C^{5+} (green) and Pd^{21+} (red) components obtained in the simulation. The energy per nucleon of the C^{5+} ions agrees well with the measured energies and the total number of ions accelerated, albeit with a somewhat smaller energy spread. The energy spectrum and peak ionization state of Pd between 50 and 200 MeV are likewise in good agreement with the data. From this simulation we can also infer a source layer thickness of ~10 Å (that is, a few monolayers), which is in good agreement with published measurements—for example, using Auger spectroscopy[24,25]. In our parametric simulation study, increasing the number of initial carbon layers while keeping the density fixed leads to two effects, shown in Fig. 3. The mean energy of the C^{5+} beam decreases and the energy spread increases with increased layer thickness. This trend continues until adequate space charge exists in the carbon layer to shield the ionizing electric field experienced by the carbon ions at the back of the layer. These more deeply buried carbon ions only attain ionization state C^{4+} and they separate from the layer of C^{5+} ions; for the parameters considered in this study, this occurs for areal charge densities exceeding $\sim 2 \times 10^{-8}\,\mathrm{g\,cm^{-2}}$, corresponding to a layer thickness of ~80 Å and above. Lower carbon ionization states appear with increasing layer thickness, and the ion energies eventually approach a maxwellian distribution. This behaviour is also seen in the experiment (Fig. 2). The grey curve shows the C^{4+} spectrum from a laser shot of comparable energy but from a tungsten target, which is not a catalyst for the required surface chemistry, and therefore does not form a thin source layer.

Measurements using transmission electron microscopy (see Supplementary Information section SI_4) reveal that upon heating, the target actually forms a 400-Å-thick tungsten carbide (W_2C) layer. This surface layer is not thin enough, and as a consequence the C spectrum is maxwellian and all lower charge states are present, as observed in earlier experiments[6]. Comparison of the two spectra shows that the direct production of monoenergetic ions by thin source layers is more effective than just slicing the equivalent energy range out of the maxwellian spectrum. Specifically, the number of ions in the corresponding energy range from 2.5 to 3.5 MeV per nucleon is a factor of 2 lower than in the monoenergetic case. Comparison with a cold Pd target shot at similar laser conditions also shows a maxwellian distribution of considerable lower energy (magenta curve, Fig. 2), because (1) the protons drain energy; and (2) the localized source layer is not formed. Our model predicts that the energy spread in the carbon beam may be minimized by localizing the initial carbon layer spatially, that is, by minimizing the source layer thickness, a process which should also result in higher mean energy of the light ion beam. This hypothesis will be tested in future experiments.

Our experimental results, simulation and analytic modelling have established the basis for laser-driven acceleration of monoenergetic ion beams using specifically designed and treated targets. Moreover, catalytic metal substrates such as Pd offer the chance of having a target that configures itself *in situ* if subjected to the right conditions. Such a target would solve major technical obstacles for a host of possible applications, making future laser-based accelerators much more feasible. We recently confirmed these results by repeating the experiments in another campaign at the Trident facility, using a substantially equivalent experimental set-up, where we reproduced the qualitative findings reported here. Although the errors in the analysis for any specific shot are small, the reproducibility of our C^{5+} results from shot to shot is only ~50%, possibly owing to the degree of control and diagnosis of key input parameters achievable in our present experimental set-up. Large, high-energy, single-shot glass lasers have typical shot-to-shot power fluctuations of ~25%, and the focal spot conditions drift over time. Varying preplasma conditions and possible self-focusing add further to the variability of the results.

The resulting unique beam characteristics, including short pulse duration, high current and small transverse and longitudinal emittances, represent a strong incentive to pursue further research and applications, such as advanced accelerator concepts[11], laboratory astrophysics, isochoric heating[21], fusion science[15] and medical physics[14]. The achieved particle energy is already in the right energy range for fusion applications like fast ignition, whereas particle number and conversion efficiency have to be substantially increased. For medical applications like tumour therapy the situation is the opposite: here, the particle numbers are sufficient but the particle energy has to be increased substantially. Considering the fast paced progress in ultrahigh intensity laser technology in recent years, it is reasonable to anticipate progress on all these issues and the deployment of a laser-driven, quasi-monoenergetic ion accelerator in the not so distant future. Progress made in diode-pumped glass laser systems, especially, should enable far higher repetition rates of 0.1–1 Hz (ref. 26). At these repetition rates, several applications in accelerator physics, medical physics, material science and neutron physics become feasible.

METHODS

Laser system and diagnostics. The experiments were performed at the short pulse arm of the Trident Nd:glass laser facility at Los Alamos National Laboratory. The Trident C-beam delivers up to 30 TW in a 20 J, ~600 fs pulse at 1.054 μm wavelength, using chirped pulse amplification[27]. The typical pulse contrast is $\sim 10^{-6}$ at 2 ns before the peak of the pulse. As illustrated in Fig. 1, an off-axis parabolic mirror is used to focus the laser pulse onto a thin foil target at 22.5° with respect to the target normal. Typical focal spot sizes are ~10 μm radius, resulting in intensities on target of $\sim 10^{19}\,\mathrm{W\,cm^{-2}}$. A stack of Gafcom radiochromic film (RCF) is placed behind the target to record the ion beam profile. A hole in the middle of this film stack provides a line of sight for a Thomson parabola (TP) ion spectrometer[28] attached to the outer chamber wall. The Thomson parabola deflects the ions by means of parallel electric and magnetic fields, so that the projection of their path in the detector is defined by parabolic traces. Ions with different charge-to-mass ratios are deflected onto different traces, while their positions on a given trace are determined by their energies. A CR-39 solid state nuclear track detector records the ions, typically ~300,000 per shot, and is read out by a specialized automated analysis system[29]. With properly chosen parameters, the counting error is below 0.01%. The error in ion numbers per energy bin (dN) is dominated by Poisson statistics, and is below ≤1% owing to the large number of counts per shot. For example, for the C^{5+} trace in Fig. 2, $dN \approx 0.3\%$. The solid angles of the TPs are 3.4×10^{-5} millisteradians (msr), and the opening angles of the ion beams are 24–100 msr depending on charge state and energy. The TPs are absolutely calibrated for energy and the energy error is dominated by the pinhole size (100 μm). It is given as $dE \sim E^{3/2}$, yielding an upper boundary for an energy error of less than 1 MeV for ~45 MeV carbon, that is, less than 2% and decreasing with energy.

Target treatment and chemistry. The foil target is heated to $T_t \approx 1{,}100$ K by two attached wires that pass a current through the foil. Palladium at room temperature is a hydrogen-getter, that is, H can be found throughout the bulk of the material as well as on the surfaces. The heating process desorbs the hydrogen contaminants (adsorbed and absorbed in the foil), thus enabling the efficient acceleration of heavier ions. In the experiment presented here, the special

catalytic surface chemistry of palladium causes a few carbon monolayers of hydrocarbon contaminants to remain on the surface of the palladium substrate and form a well defined source layer for the monoenergetic carbon beam. Given the ambient vacuum of $\sim 10^{-6}$ mbar, the surface is contaminated with various C_xH_y compounds. When the Pd is heated, the Pd surface undergoes multiple phase changes[24,25] and the loosely bound H is driven out of the bulk and off the surfaces. At 600 K the target is completely dehydrogenized. The carbon, however, remains on the surface in various different configurations. When heating the target further, to temperatures $T > 1{,}100$ K, the various carbon compounds undergo a phase change, forming a well-defined, very thin graphite layer at the monolayer scale on the Pd surface. If heated up further, to above 1,300 K, this layer will be removed and a clean Pd surface remains. In the experiment, we did not reach this last state, but remained in the graphite regime, thereby preparing a thin source layer perfect for creating monoenergetic ions.

BILBO hybrid code. In BILBO, ion formation and acceleration is accomplished by the electric fields of a virtual cathode of hot electrons at the back surface of the target. Assuming separation of the electron and ion timescales, self-consistent electric fields are obtained by solving the time-stationary relativistic Vlasov–Maxwell equations for each electron component. These fields accelerate the ions and ionize them to higher charge states, where ionization is implemented in BILBO by means of a threshold ionization model[30]. The boundary conditions require the electric field to vanish within the target and far from the target surface. In addition, the electron densities and temperatures of the hot and cold components are specified within the target as internal boundary conditions. The hot electron density and temperature are functions of the laser energy deposition model, and their dynamics include adiabatic expansion and the loss of energy to ionization and ion acceleration. The cold electron temperature increases from ohmic heating and collisions with the hot electron component. In the simulations, the laser spot diameter was assumed to be 30 μm; 50% absorption of the incident laser into hot electrons was assumed ($T_h \approx 2.5$ MeV), with the hot electrons' density assumed to be equal to the critical density ($n_e = 1.01 \times 10^{21}$). The cold electrons had $n_c = 6.8 \times 10^{22}$ cm^{-3} and initial cold electron temperature $T_c = 10$ eV. The density and temperature profiles of the hot electron component were assumed to evolve in time with gaussian shape during the pulse rise and have a full-width at half-maximum of 700 fs. The simulation used 5×10^4 simulation ions of each species, had a time step of 2 fs, and employed 6×10^5 simulation cells over a domain of size 100 μm.

Received 17 August; accepted 3 November 2005.

1. Katsouleas, T. Accelerator physics: Electrons hang ten on laser wake. *Nature* **431,** 515–516 (2004).
2. Faure, J. *et al.* A laser–plasma accelerator producing monoenergetic electron beams. *Nature* **431,** 541–544 (2004).
3. Mangles, S. *et al.* Monoenergetic beams of relativistic electrons from intense laser–plasma interactions. *Nature* **431,** 535–538 (2004).
4. Geddes, C. *et al.* High-quality electron beams from a laser wakefield accelerator using plasma-channel guiding. *Nature* **431,** 538–541 (2004).
5. Hatchett, S. *et al.* Electron, photon, and ion beams from the relativistic interaction of Petawatt laser pulses with solid targets. *Phys. Plasmas* **5,** 2076–2082 (2000).
6. Hegelich, M. *et al.* MeV ion jets from short-pulse-laser interaction with thin foils. *Phys. Rev. Lett.* **89,** 085002 (2002).
7. Roth, M. *et al.* Energetic ions generated by laser pulses: A detailed study on target properties. *Phys. Rev. Spec. Topic Accelerators Beams* **5,** 061002 (2002).
8. Snavely, R. *et al.* Intense high-energy proton beams from petawatt-laser irradiation of solids. *Phys. Rev. Lett.* **85,** 2945–2948 (2000).
9. Maksimchuk, A., Gu, S., Flippo, K., Umstadter, D. & Bychenkov, V. Yu. Forward ion acceleration in thin films driven by a high-intensity laser. *Phys. Rev. Lett.* **84,** 4108–4111 (2000).
10. Cowan, T. *et al.* Ultralow emittance, multi-MeV proton beams from a laser virtual-cathode plasma accelerator. *Phys. Rev. Lett.* **92,** 204801 (2004).
11. Habs, D., Pretzler, G., Pukhov, A. & Meyer-ter-Vehn, J. Laser acceleration of electrons and ions and intense secondary particle generation. *Prog. Part. Nucl. Phys.* **46,** 375–377 (2001).
12. Cobble, J. A., Johnson, R. P., Cowan, T. E., Renard-Le Galloudec, N. & Allen, M. High resolution laser-driven proton radiography. *J. Appl. Phys.* **92,** 1775–1779 (2002).
13. Borghesi, M. *et al.* Proton imaging: a diagnostic for inertial confinement fusion/ fast ignitor studies. *Plasma Phys. Control Fusion* **43,** A267–A276 (2001).
14. Ledingham, K. *et al.* High power laser production of short-lived isotopes for positron emission tomography. *J. Phys. D* **37,** 2341–2345 (2004).
15. Kodama, R. *et al.* Fast heating of ultrahigh-density plasma as a step towards laser fusion ignition. *Nature* **412,** 798–802 (2001).
16. Roth, M. *et al.* Fast ignition by intense laser-accelerated proton beams. *Phys. Rev. Lett.* **86,** 436–439 (2001).
17. Temporal, M., Honrubia, J. J. & Atzeni, S. Numerical study of fast ignition of ablatively imploded deuterium–tritium fusion capsules by ultra-intense proton beams. *Phys. Plasmas* **9,** 3098–3107 (2002).
18. Wilks, S. *et al.* Energetic proton generation in ultra-intense laser–solid interactions. *Phys. Plasmas* **8,** 542–549 (2001).
19. Atzeni, S. & Meyer-ter-Vehn, J. *The Physics of Inertial Confinement Fusion* (Oxford Univ. Press, Oxford, 2004).
20. Hegelich, M. *et al.* Spectral properties of laser-accelerated mid-Z MeV/u ion beams. *Phys. Plasmas* **12,** 056314 (2005).
21. Patel, P. *et al.* Isochoric heating of solid-density matter with an ultrafast proton beam. *Phys. Rev. Lett.* **91,** 125004 (2003).
22. Gitomer, S. J. *et al.* Fast ions and hot electrons in the laser-plasma interaction. *Phys. Fluids* **29,** 2679–2688 (1986).
23. Esirkepov, T. Zh. *et al.* Proposed double-layer target for the generation of high-quality laser-accelerated ion beams. *Phys. Rev. Lett.* **89,** 175003 (2002).
24. Hamilton, J. C. & Blakeley, J. M. Carbon segregation to single crystal surfaces of Pt, Pd and Co. *Surf. Sci.* **91,** 199–217 (1980).
25. Ramsier, R. D., Lee, K.-W. & Yates, J. T. Jr A sensitive method for measuring adsorbed carbon on palladium surfaces: Titration by NO. *J. Vac. Sci. Technol.* **13,** 188–194 (1995).
26. Hein, J. *et al.* Diode-pumped chirped pulse amplification to the joule level. *Appl. Phys. B* **79,** 419–422 (2004).
27. Mourou, G. A. & Umstadter, D. Extreme light. *Sci. Am.* **286,** 80–86 (2002).
28. Thomson, J. J. Rays of positive electricity. *Phil. Mag.* **21,** 225–249 (1911).
29. Rusch, G., Winkel, E., Noll, A. & Heinrich, W. The Siegen automatic measuring system for track detectors: New developments. *Nucl. Tracks Radiat. Meas.* **19,** 261–265 (1991).
30. Augst, S., Meyerhofer, D. D., Strickland, D. & Chint, S. L. Laser ionization of noble gases by Coulomb-barrier suppression. *J. Opt. Soc. Am. B* **8,** 858–867 (1991).

Supplementary Information is linked to the online version of the paper at www.nature.com/nature.

Acknowledgements We acknowledge the expert support of the Trident laser team, especially R. Johnson, T. Ortiz and R. Gonzales, and the target fabrication support from LANL group MST-7, particularly R. Perea. This work was supported by the LANL Laboratory Directed Research & Development (LDRD) programme. One of the authors (H.R.) was supported by DOE/NNSA-UNR and another (J.S.) by DFG and BMBF.

Author Contributions B.M.H. conceived the experiment, B.M.H., J.C., S.L. and J.C.F. executed the experiment, B.M.H., J.S., K.F. and J.C.F. analysed the data, H.R., B.J.A. and B.M.H. did the theory, M.P. and R.K.S. helped with the material science part and palladium surface chemistry, and B.M.H., B.J.A. and J.C.F. wrote the paper.

Author Information Reprints and permissions information is available at npg.nature.com/reprintsandpermissions. The authors declare no competing financial interests. Correspondence and requests for materials should be addressed to B.M.H. (hegelich@lanl.gov).